Published in final edited form as:
Magn Reson Med. 2009 February ; 61(2): 481–485. doi:10.1002/mrm.21823.

Magnetic Field Correlation as a Measure of Iron-Generated Magnetic Field Inhomogeneities in the Brain

Jens H. Jensen[1], **Kamila Szulc**[1], **Cathy Hu**[1], **Anita Ramani**[1], **Hanzhang Lu**[1], **Liang Xuan**[1], **Maria F. Falangola**[1,2], **Ramesh Chandra**[1], **Edmond A. Knopp**[1], **John Schenck**[3], **Earl A. Zimmerman**[4], and **Joseph A. Helpren**[1,2]

[1]Center for Biomedical Imaging, Department of Radiology, New York University School of Medicine, New York, New York

[2]Center for Advanced Brain Imaging, The Nathan Kline Institute, Orangeburg, New York

[3]General Electric Global Research Center, Schenectady, New York

[4]Department of Neurology, Albany Medical College, Albany, New York

Abstract

The magnetic field correlation (MFC) at an applied field level of 3 T was estimated by means of MRI in several brain regions for 21 healthy human adults and one subject with aceruloplasminemia. For healthy subjects, highly elevated MFC values compared to surrounding tissues were found within the basal ganglia. These are argued as being primarily the result of microscopic magnetic field inhomogeneities generated by non-heme brain iron. The MFC in the aceruloplasminemia subject was significantly higher than for healthy adults in the globus pallidus, thalamus and frontal white matter, consistent with the known increased brain iron concentration associated with this disease.

Keywords

magnetic field correlation; brain; iron; magnetic field inhomogeneities; aceruloplasminemia; MRI

INTRODUCTION

The strong applied magnetic field produced inside a typical MRI scanner can magnetize biological tissues to the extent that they generate significant static magnetic field perturbations of several parts per million (1). These field perturbations are often spatially inhomogeneous, both due to tissue geometry and the heterogeneous magnetic properties of many tissues. In considering their MRI effects, it is convenient to categorize such induced static magnetic field inhomogeneities (MFIs) as either macroscopic or microscopic according to whether they vary on a length scale large or small compared to the dimensions of a voxel.

Macroscopic MFIs are chiefly attributable to magnetic susceptibility discontinuities associated with tissue-air and tissue-tissue interfaces and hence reflect gross anatomy. They may be problematic for MRI, causing image distortion, but can also provide a useful contrast mechanism, as exemplified by susceptibility-weighted imaging (2). Moreover,

*Correspondence to: Jens H. Jensen, Department of Radiology, New York University School of Medicine, KIP-600-A, 650 First Avenue, New York, NY 10016-3240. Email: jens.jensen@med.nyu.edu; Tel.: (212)263-6605; FAX: (212)263-7541.

macroscopic MFIs can be quantified with field maps that are measurable by MRI using well-established methods based on phase images (3,4).

Microscopic MFIs, on the other hand, are mainly a consequence of subvoxel structures not resolvable with MRI. Nonetheless, microscopic MFIs can have a substantial effect on the MR relaxations rates R_2 and R_2^*, and signal changes observed in functional MRI of the brain due to the blood-oxygen-level-dependent (BOLD) effect are due, at least in part, to microscopic MFIs produced by deoxyhemoglobin within small blood vessels (5,6).

The magnetic field correlation (MFC) provides a quantitative measure of MFIs that can be estimated with MRI (7). In contrast to a field map, the MFC contains information about both macroscopic and microscopic MFIs. It differs from R_2 and R_2^* in having a simpler and more direct connection to MFIs and in being, by definition, independent of relaxation mechanisms, such as dipolar interactions, unrelated to MFIs (7).

The central purpose of this article is to give evidence that the MFC in certain brain regions, at an applied field level of 3 T, is determined primarily by microscopic MFIs generated by non-heme iron and thereby to support the application of MFC imaging to the study of iron changes associated with neuropathology. Non-heme iron plays a critical role in cerebral metabolism and has been linked to a number of brain disorders, including Parkinson's and Alzheimer's diseases (8), and the sensitivity of R_2 and R_2^* to brain iron has been investigated in several prior MRI studies (9–13).

We present MFC measurements for 21 healthy subjects and one subject with aceruloplasminemia, a rare iron overload disorder distinguished by a highly elevated brain iron concentration (14,15). These data are compared with published values for the iron concentration in selected brain regions.

THEORY

MFC imaging

The MFC of a biological tissue in the applied magnetic field of an MRI scanner is defined by

$$\mathrm{MFC}(t) \equiv \gamma^2 C(t) \qquad [1]$$

where $\gamma = 2.675 \times 10^8\ \mathrm{s^{-1}T^{-1}}$ is the proton gyromagnetic ratio and C is the correlation function given by

$$C\left(\left|t - t'\right|\right) \equiv \left\langle \delta B\,(t)\, \delta B\left(t'\right)\right\rangle \qquad [2]$$

with $\delta B(t)$ being the difference between the magnitude of the total magnetic field experienced by a water molecule at a time t and the magnitude of the uniform background field. The angle brackets in Eq. [2] indicate an averaging over all the water molecules within a voxel, and the correlation function depends only on the time difference because of time translation invariance. The MFC thus provides a means of characterizing MFIs, with MFC(0) simply being proportional to the variance of the field.

The MFC can be estimated from MRI by using an asymmetric spin echo (ASE) sequence together with the formula

$$S(t;t_s+t/2) \approx S(t;t/2)\exp\left[-2t_s^2\mathrm{MFC}(t/2)\right], \quad [3]$$

where $S(t; t')$ is the signal intensity at a time t obtained with the 180° refocusing radiofrequency (RF) pulse positioned at a time t′ (7). The time t_s corresponds to the shift of the 180° RF pulse from its standard spin echo value of $t/2$. Hence, the MFC may be found by fitting the ASE signal intensity as a function of the time shift t_s to a Gaussian form.

Equation [3] is most accurate for small time shifts, but the precision of the MFC estimation is improved by using larger time shifts. Hence, in practice it is preferable to choose the smallest time shifts that provide sufficient precision for any given application. It is also important to bear in mind that the MFC is time dependent and tends to decrease monotonically with increasing echo times, as has been demonstrated in phantoms (7). This decrease is due to water diffusion, and it may thus be advantageous to minimize the time of signal acquisition in order to maximize the MFC and minimize the diffusion effect.

We note that the conventional relaxation rates of R_2, R_2^* and R_2' may also be obtained from ASE signal intensities (16). The MFC's relationship to relaxation rates and the technical distinctions in its measurement method are discussed in detail in Ref. 7.

The macroscopic contribution to the MFC is given by

$$\mathrm{MFC}_{\mathrm{mac}}=\frac{\gamma^2}{12}\left(G_x^2L_x^2+G_y^2L_y^2+G_z^2L_z^2\right) \quad [4]$$

where L_x, L_y, and L_z are the dimensions of the voxel in Cartesian x, y, z directions and G_x, G_y, and G_z are the corresponding components of the macroscopic static gradient field (7). A microscopic contribution to the MFC may then be defined by

$$\mathrm{MFC}_{\mathrm{mic}} \equiv \mathrm{MFC} - \mathrm{MFC}_{\mathrm{mac}}. \quad [5]$$

From a field map, the static gradient field (not to be confused with the imaging gradients), and thus $\mathrm{MFC}_{\mathrm{mac}}$, can be estimated by finite differences. Since the phase of the ASE signal, in radians, is given approximately by

$$\phi=2\gamma t_s B_0 \bmod 2\pi, \quad [6]$$

with B_0 being the static field strength, the same ASE sequence used to determine the MFC can also be employed to estimate both $\mathrm{MFC}_{\mathrm{mac}}$ and $\mathrm{MFC}_{\mathrm{mic}}$. There are $O\left(t_s^3\right)$ corrections to Eq. [6], and so it is most accurate for small t_s.

METHODS

Human Subjects

MFC imaging was performed on 21 healthy adult subjects (age = 34.4 ± 10.0 yrs; 11 male, 10 female) and one male subject diagnosed with aceruloplasminemia (age = 58 yrs). Only one aceruloplasminemia subject could be studied, since subject recruitment is difficult due to a low prevalence for this genetic disorder of about 1 in 2,000,000 births (14). However, the large changes in non-heme brain iron concentration associated with aceruloplasminemia

makes it ideal for testing our hypothesized link between iron and the MFC. The study was approved by the Institutional Review Board of the New York University School of Medicine and informed consent was obtained from all subjects.

MR Imaging

All experiments were conducted on a 3 T MR scanner (Trio, Siemens Medical Solutions, Erlangen, Germany). ASE images were acquired using a segmented echo planar imaging (EPI) sequence with 37 lines of phase space being obtained for each excitation (i.e., EPI factor = 37). The echo time (TE) was 46 ms, and the 180° (sinc) refocusing pulse time shifts were t_s = 0, −4, −8, −12, and −16 ms, with the negative signs indicating a reduction in the interval between the refocusing pulse and the initial 90° excitation pulse. The field of view was 256 × 256 mm^2, the slice thickness was 2 mm, the interslice gap was 2 mm, and the repetition time was 1500 ms.

In order to test the resolution dependence of the MFC estimates, healthy subjects were imaged with three different acquisition matrices of 192 × 192, 128 × 128, and 64 × 64, yielding in-plane resolutions of 1.33 × 1.33 mm^2, 2 × 2 mm^2, and 4 × 4 mm^2. The bandwidth was 1370 Hz/pixel for the 192 × 192 acquisitions, and the bandwidth was 1346 Hz/pixel for the 128 × 128 and 64 × 64 acquisitions. The aceruloplasminemia subject was only scanned with the 192 × 192 acquisition matrix.

For each healthy subject, 9 axial slices were obtained, which were located so that the central slices included the basal ganglia region. For each slice, resolution, and refocusing pulse time shift, 10 images were acquired. These were spatially co-registered with the Statistical Parametric Mapping (University College London, UK) software package run under MATLAB (Mathworks, Natick, MA, USA) and averaged prior to further processing. Both magnitude and phase information was saved.

The same procedure was followed for the aceruloplasminemia subject, using a 192 × 192 resolution, except that 19 axial slices were obtained and that only magnitude data were saved. The entire protocol was repeated twice to facilitate error estimation of the MFC values.

Data analysis

After co-registration and averaging, the ASE images were used to generate parametric maps of the MFC. For healthy subjects, MFC maps were determined from a least squares nonlinear fit to Eq. [3] with t = TE. Thus, our MFC values correspond to a time TE/2 = 23 ms, as follows from Eq. [3]. For the aceruloplasminemia subject, the same method was utilized to calculate MFC maps except that the effect of background noise was incorporated into the fitting procedure, as described in Ref. 7, due to a substantially higher transverse relaxation rate.

For healthy subjects, MFC_{mac} maps were generated from the phase images by first determining maps for the macroscopic gradient field components. As follows from Eq. [6], the phase and magnetic field strength at a position **r** can be related by

$$B_0(\mathbf{r}) = \frac{\phi(\mathbf{r}, t_s) - \phi(\mathbf{r}, t_s') + 2\pi n}{2\gamma(t_s - t_s')} \quad [7]$$

where t_s and t_s' are two different values for the refocusing pulse time shift and n is an integer that accounts for any phase wrap around. The components of the gradient field may then be

obtained by using a finite differences approximation. Wrap around ambiguities were resolved by choosing the *n* values to minimize the magnitudes of the gradient components. This assumption is valid provided the gradient fields are sufficiently small, which was verified for the brain regions investigated. Maps for the gradient field components were obtained using both the choice t_s = 4 ms and t_s'=0 ms and the choice t_s = 8 ms and t_s'=4 ms. From the geometric mean of the two gradient field maps for each component, average gradient field maps were calculated. A geometric mean was used rather than an arithmetic mean in order to obtain an unbiased estimation for MFC_{mac}.

The MFC_{mic} maps were simply calculated by subtracting the MFC and MFC_{mac} maps, as suggested by Eq. [5]. The MFC, MFC_{mac}, and MFC_{mic} maps for the 128 × 128 and 64 × 64 acquisitions were interpolated to 192 × 192 and co-registered with the maps for the 192 × 192 acquisition. Regions of interest (ROI) were drawn manually on the ASE images acquired with the 192 × 192 matrix and t_s = 0 ms (i.e., conventional spin echo images). The selected ROI corresponded to samples from the globus pallidus (GP), putamen (PU), head of the caudate nucleus (CN), thalamus (TH), and frontal white matter (FW). All ROI were rectangular in shape and for a given tissue type situated on a single slice, with dimensions adjusted according to the targeted structure's size and shape.

In order to assess how strongly the MFC correlates with expected non-heme iron concentrations, the measured MFC, MFC_{mac}, and MFC_{mic} for the healthy subjects were compared to values cited in the classic study of Hallgren and Sourander (17) that gives average iron concentrations in selected brain regions based on chemical analysis of postmortem brain tissue.

RESULTS

Healthy subjects

A representative spin echo (i.e., t_s = 0 ms) image obtained with a 192 × 192 acquisition matrix together with its corresponding MFC, MFC_{mac}, and MFC_{mic} maps are shown in Fig. 1. Both MFC and MFC_{mic} are clearly elevated within the basal ganglia relative to the surrounding tissue. MFC_{mac} is substantially smaller within most of the brain except for the hypointense region indicated by a horizontal arrow. Similar localized regions with large MFC_{mac} were observed in all healthy subjects. Regions with high MFC_{mac} were also often observed near the ear canals. Within the globus pallidus, the MFC and MFC_{mic} maps were, in most cases, distinctly heterogeneous, suggestive of a higher MFC in the GP interna than in the GP externa.

In Fig. 2, MFC_{mic} and MFC_{mac} for our selected ROI are plotted as a function of the in-plane resolution. MFC_{mic} is roughly independent of the resolution, consistent with its interpretation as reflecting primarily intravoxel MFIs, although the MFC_{mic} for a resolution of 4 × 4 mm^2 resolution was about 50% lower in FW than the corresponding values for resolutions of 1.33 × 1.33 mm^2 and 2 × 2 mm^2. MFC_{mac} increases linearly with the in-plane resolution, as is predicted by Eq. [4].

The measured MFC, MFC_{mic}, and MFC_{mac} values for the 1.33 × 1.33 mm^2 resolution are plotted in Fig. 3 as functions of the regional iron concentrations as given by Ref. 17. A high linear correlation is found for both MFC and MFC_{mic}, with coefficients of determination of R^2 = 0.980 and 0.983, respectively. MFC_{mac} also demonstrates a linear correlation with iron, but with a substantially lower R^2 value of 0.818.

Aceruloplasminemia subject

A spin echo image with the corresponding MFC map from the dataset for the aceruloplasminemia subject is shown in Fig 4. Compared to healthy subjects, the MFC is several times higher in most brain regions, as is particularly noticeable in cortical gray matter. MFC estimates could not be obtained for the PU and CN, since the transverse relaxation time is so short that the signal in these regions decayed to nearly the noise level prior to the signal readout. (The MFC may have been measurable in the PU and CN if smaller TE and time shifts had been employed, but then the results would not be directly comparable to those for the healthy subjects.)

Figure 5 gives a quantitative comparison of the MFC for the aceruloplasminemia subject with the mean values for the healthy subjects. The MFC is significantly elevated ($p < 0.01$) in the GP, TH, and FW. Compared to healthy subjects, the MFC for the aceruloplasminemia subject was about 5 times higher in the GP, 10 times higher in the TH, and 4 times higher in the FW. These increases are comparable to the 5 to 10 fold iron concentration increases for the GP and TH reported by Miyajima and co-workers (14). The high MFC values observed in cortical gray matter are also qualitatively consistent with iron changes associated with aceruloplasminemia (15).

DISCUSSION

For maps derived from ASE images obtained with a 192 × 192 acquisition matrix, the MFC_{mac} values are, in all the ROI considered, substantially smaller than the MFC_{mic} values, as is evident from Fig. 2 and Fig. 3, implying the MFC, for $t = 23$ ms, to be primarily due to microscopic MFIs. This holds in most other brain regions as well, with the exception of a few localized areas with elevated MFC_{mac} values, as is illustrated by Fig. 1. Probable sources of such high MFC_{mac} values are air cavities associated with the paranasal sinuses and ear canals. High MFC_{mac} values could also conceivably be generated by large blood veins, calcifications, and subject specific sources of magnetic field gradients such as dental work.

The main purpose for obtaining MFC_{mic} and MFC_{mac} maps with different resolutions was to test whether their resolution dependences are consistent with theoretical expectations. MFC_{mic} should mainly reflect MFIs with length scales smaller than the voxel size that are generated by intravoxel microscopic magnetic field perturbers. Thus, mean MFC_{mic} values should not depend strongly on the resolution, as is confirmed experimentally (Fig. 2a). MFC_{mac}, in contrast, is due to MFIs with length scales large compared to the voxel size and has an explicit dependence on the voxel dimensions as indicated by Eq. [4]. For our experiment, Eq. [4] predicts that MFC_{mac} should increase linearly with the in-plane resolution, in good agreement with our experimental observations (Fig. 2b). These results support the ability of our MR approach to decompose the MFC into microscopic and macroscopic components.

The good linear correlation between the MFC and estimated non-heme iron concentrations shown in Fig. 3 supports the view that the MFC, at least within the basal ganglia, is primarily due to non-heme iron. This is not surprising given the known high concentration of non-heme iron in these regions (17) and the fact that histological studies indicate a high density of iron-rich structures consisting of both individual cells and cell clusters (18). However, it is conceivable hat a blood contribution may also be significant for some brain regions with lower MFC values ($<100\ s^{-2}$ for $B_0 = 3$ T).

The regional MFC values reported here are similar to those previously reported (19,20). However, it is important to emphasize that the methodologies employed in these prior

studies are significantly different from that used here, and a close correspondence cannot necessarily be expected. Key differences that may influence MFC estimation include image resolution, echo time, ROI delineation, and EPI factor (since ghosting and T_2^* blurring are potential sources of MFC errors).

The results for the aceruloplasminemia subject provide further support for a strong link between MFC and non-heme brain iron, since measured MFC values are elevated relative to those of healthy adults in similar way as prior studies have shown for iron (14,15). These also illustrate the potential applicability of MFC imaging in the study of neuropathology.

Acknowledgments

We thank Glyn Johnson and Dan Kim for useful discussions and Edgar Suan for helping to organize the experimental studies. This work was supported in part by grants from the National Institutes of Health (NIBIB R21/R33EB003305, NIA R01AG027852, NINDS R01NS039135) and by the Litwin Fund for Alzheimer's Research.

REFERENCES

1. Schenck JF. The role of magnetic susceptibility in magnetic resonance imaging: MRI magnetic compatibility of the first and second kinds. Med Phys. 1996; 23:815–850. [PubMed: 8798169]
2. Haacke EM, Xu Y, Cheng YC, Reichenbach JR. Susceptibility weighted imaging (SWI). Magn Reson Med. 2004; 52:612–618. [PubMed: 15334582]
3. Reber PJ, Wong EC, Buxton RB, Frank LR. Correction of off resonance-related distortion in echo-planar imaging using EPI-based field maps. Magn Reson Med. 1998; 39:328–330. [PubMed: 9469719]
4. Ogg RJ, Langston JW, Haacke EM, Steen RG, Taylor JS. The correlation between phase shifts in gradient-echo MR images and regional brain iron concentration. Magn Reson Imaging. 1999; 17:1141–1148. [PubMed: 10499676]
5. Yablonskiy DA, Haacke EM. Theory of NMR signal behavior in magnetically inhomogeneous tissues: the static dephasing regime. Magn Reson Med. 1994; 32:749–763. [PubMed: 7869897]
6. Boxerman JL, Hamberg LM, Rosen BR, Weisskoff RM. MR contrast due to intravascular magnetic susceptibility perturbations. Magn Reson Med. 1995; 34:555–566. [PubMed: 8524024]
7. Jensen JH, Chandra R, Ramani A, Lu H, Johnson G, Lee SP, Kaczynski K, Helpern JA. Magnetic field correlation imaging. Magn Reson Med. 2006; 55:1350–1361. [PubMed: 16700026]
8. Schenck JF, Zimmerman EA. High-field magnetic resonance imaging of brain iron: birth of a biomarker? NMR Biomed. 2004; 17:433–445. [PubMed: 15523705]
9. Gelman N, Gorell JM, Barker PB, Savage RM, Spickler EM, Windham JP, Knight RA. MR imaging of human brain at 3.0 T: preliminary report on transverse relaxation rates and relation to estimated iron content. Radiology. 1999; 210:759–767. [PubMed: 10207479]
10. Bartzokis G, Tishler TA, Lu PH, Villablanca P, Altshuler LL, Carter M, Huang D, Edwards N, Mintz J. Brain ferritin iron may influence age- and gender-related risks of neurodegeneration. Neurobiol Aging. 2007; 28:414–423. [PubMed: 16563566]
11. Schenck JF, Zimmerman EA, Li Z, Adak S, Saha A, Tandon R, Fish KM, Belden C, Gillen RW, Barba A, Henderson DL, Neil W, O'Keefe T. High-field magnetic resonance imaging of brain iron in Alzheimer disease. Top Magn Reson Imaging. 2006; 17:41–50. [PubMed: 17179896]
12. House MJ, St Pierre TG, Foster JK, Martins RN, Clarnette R. Quantitative MR imaging R2 relaxometry in elderly participants reporting memory loss. AJNR Am J Neuroradiol. 2006; 27:430–439. [PubMed: 16484425]
13. Mitsumori F, Watanabe H, Takaya N, Garwood M. Apparent transverse relaxation rate in human brain varies linearly with tissue iron concentration at 4.7 T. Magn Reson Med. 2007; 58:1054–1060. [PubMed: 17969101]
14. Miyajima H, Takahashi Y, Kono S. Aceruloplasminemia, an inherited disorder of iron metabolism. Biometals. 2003; 16:205–213. [PubMed: 12572680]

15. Kono S, Miyajima H. Molecular and pathological basis of aceruloplasminemia. Biol Res. 2006; 39:15–23. [PubMed: 16629161]
16. Ma J, Wehrli FW. Method for image-based measurement of the reversible and irreversible contribution to the transverse-relaxation rate. J Magn Reson B. 1996; 111:61–69. [PubMed: 8620286]
17. Hallgren B, Sourander P. The effect of age on the non-haemin iron in the human brain. J Neurochem. 1958; 3:41–51. [PubMed: 13611557]
18. Connor JR, Menzies SL, St Martin SM, Mufson EJ. Cellular distribution of transferrin, ferritin, and iron in normal and aged human brains. J Neurosci Res. 1990; 27:595–611. [PubMed: 2079720]
19. Ramani A, Jensen JH, Kaczynski KR, Helpern JA. In-vivo magnetic field correlation imaging of human brain at 3 Tesla. Proc Intl Soc Mag Reson Med. 2005; 13:2177.
20. Ge Y, Jensen JH, Lu H, Helpern JA, Miles L, Inglese M, Babb JS, Herbert J, Grossman RI. Quantitative assessment of iron accumulation in the deep gray matter of multiple sclerosis by magnetic field correlation imaging. AJNR Am J Neuroradiol. 2007; 28:1639–1644. [PubMed: 17893225]

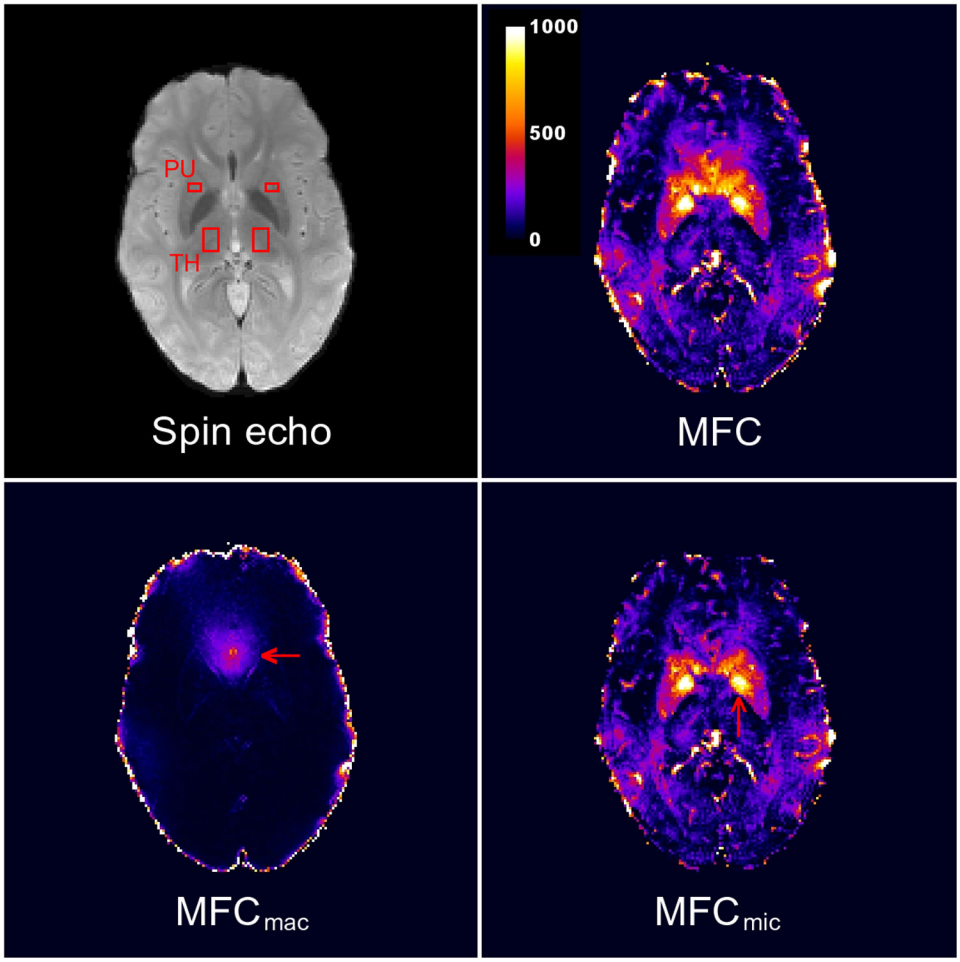

1.

Representative images and parametric maps from a single, healthy subject obtained with a 192 × 192 acquisition matrix. The spin echo image corresponds to $t_s = 0$ (i.e., a standard spin echo) and illustrates typical ROI for the PU and TH used in the data analysis. The MFC map shows an elevated MFC in the basal ganglia, as well as near large blood veins. The macroscopic contribution to the MFC is revealed by the MFC_{mac} map and is dominated by a single feature (indicated by horizontal arrow), which may be plausibly attributed MFIs generated by the paranasal sinuses. The MFC_{mic} map, determined from the difference between MFC and MFC_{mac} maps, shows the contribution to the MFC from MFIs varying on smaller length scales. Note that MFC_{mic} within the GP appears to be distinctly heterogeneous with hyperintense subregions (indicated by vertical arrow). The calibration bar for the maps is labeled in units of s^{-2}.

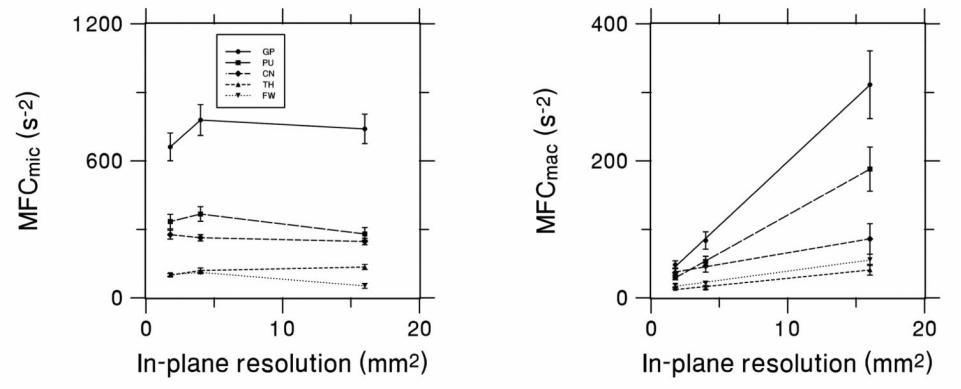

2.

Effect of changing the in-plane image resolution on average values from 21 healthy adults for (a) MFC_{mic} and (b) MFC_{mac}. The smallest, intermediate and largest resolutions correspond to 192 × 192, 128 × 128, and 64 × 64 acquisition matrices, respectively. The field of view and slice thickness are the same for all three cases. In (a), the lines are guides for the eye, while in (b) they are least squares linear fits. MFC_{mic} is approximately independent of the resolution supporting its interpretation as representing the microscopic component of the MFC, while MFC_{mac} increases linearly with the resolution as expected for the macroscopic component. The error bars indicate standard error estimates.

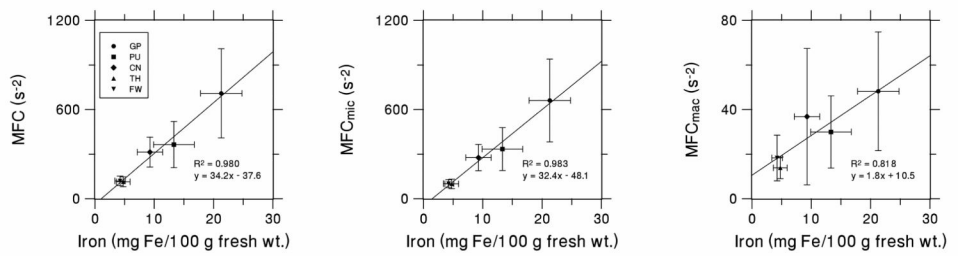

3.

Average values for (a) MFC, (b) MFC_{mic}, and (c) MFC_{mac} in selected brain regions versus estimated non-heme iron concentrations for 21 healthy adults. Iron concentrations are taken from Ref. 17. The strong linear correlations are consistent with the MFC being significantly affected by the presence of iron. Note the different *y*-axis scale in (c). The error bars represent standard deviations.

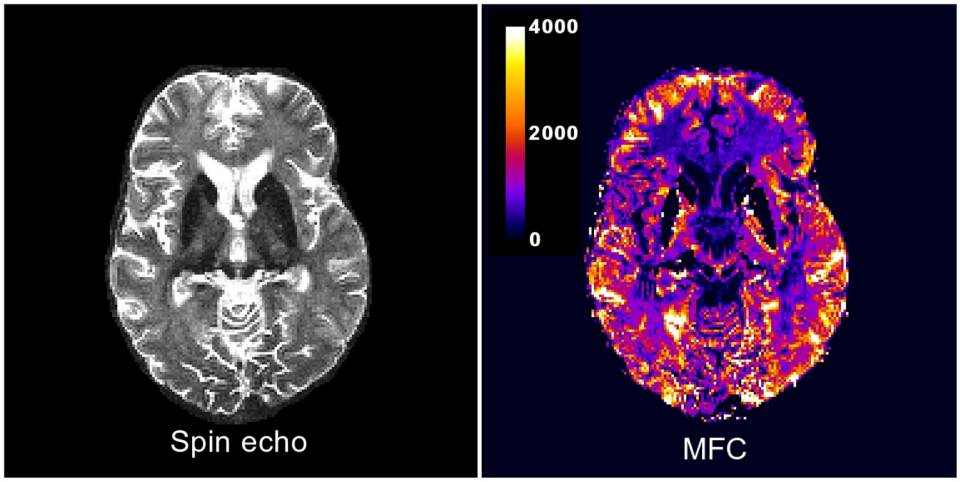

4.

Spin echo image and the corresponding MFC map for aceruloplasminemia subject. Highly elevated MFC values are apparent throughout most of the brain. Signal voids in the PU and CN are the result of very rapid transverse relaxation in these regions. The calibration bar for the MFC map is labeled in units of s^{-2}.

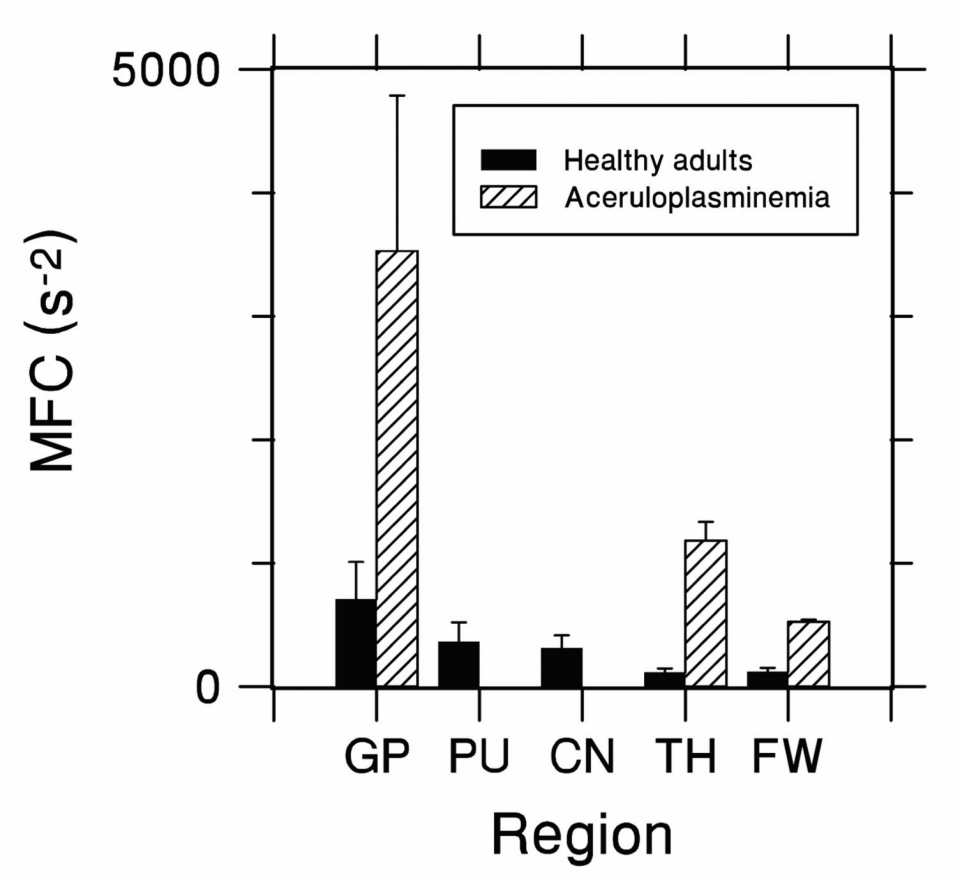

5.

Comparison of MFC values in selected brain regions for healthy adults and the aceruloplasminemia subject. MFC values in the PU and CN could not be obtained for the aceruloplasminemia subject due to low signal in these regions. The significantly higher MFC values in the GP, TH and FW for the aceruloplasminemia subject are consistent with the MFC being an indicator of non-heme brain iron concentration. The error bars represent standard deviations. For the aceruloplasminemia subject, the standard deviations were calculated by using data from two separate trials.